Experimental and simulation results of OBIC Technique Applied to Wide Bandgap Semiconductors

Dominique Planson, Luong-Viet Phung, Besar Asllani, Pascal Bevilacqua, Hassan Hamad, Christophe Raynaud

Experimental and simulation results of OBIC Technique Applied to Wide Bandgap Semiconductors

Dominique Planson, Luong-Viet Phung, Besar Asllani, Pascal Bevilacqua, Hassan Hamad, Christophe Raynaud

Univ Lyon, INSA Lyon, Ecole Centrale de Lyon, Université Claude Bernard Lyon 1, CNRS, Ampère, F-69621, Villeurbanne, France

*dominique.planson@insa-lyon.fr

Abstract

Power electronic devices based on wide bandgap (WBG) semiconductors (like silicon carbide (SiC), gallium nitride (GaN), diamond (C) ...) offer better performances when compared to those based on silicon (Si). However, the periphery protection of these devices must be carefully designed to sustain high voltage bias. This paper shows how the OBIC (Optical Beam Induced Current) technique applied to WBG semiconductor devices could be useful to study the efficiency of different protection techniques. Firstly, a theoretical approach is given to present the method. Then, this electro-optical characterization technique is performed on high voltage power devices in a vacuum chamber allowing to study the spatial distribution of the electric field in the semiconductor. Results are mainly focused on SiC devices for the sake of availability. Finally, comparisons with Finite Elements Methods using TCAD tools are performed showing the local high electric field strength.

This paper shows also additional results and measurements on GaN and diamond Schottky diodes. Finally, extraction of OBIC signals allows to know some physical features as shown in the last section like ionization coefficients, minority carrier lifetime and local defects in semiconductors.

Keywords: optical device characterization, power devices, Silicon Carbide, Gallium Nitride, Diamond.

1 Introduction

Wide Bandgap semiconductors materials like Silicon Carbide (SiC) Gallium Nitride (GaN) and Diamond (C) have excellent properties for many applications especially for high voltage devices [1][2][3].

Future smart grids and HVDC (High Voltage Direct Current) transmission energy topologies will soonly require ultrahigh voltage devices (>10 kV) [4][5][6]. In order to fully benefit the advantages of WBG semiconductors materials and avoid premature breakdown of the high voltage devices, it is mandatory to have efficient periphery protections [7][8]. This paper will show how the OBIC techniques could help determining the efficiency of the periphery protection by analyzing the electric field distribution in the structure and especially at the junction periphery. A comparable technique to OBIC is EBIC (Electron Beam Induced Current). It enables the quick and accurate characterization of local electric field in the device where the built-in potential exists, but it is not applicable with high voltage biased device.

2 OBIC principle

A focused laser beam is used to generate electron-hole pairs (EHPs) into the semiconductor as shown in Fig. 1 for an infinite plane-parallel PN junction. Two semi-reflecting mirrors and a focusing lens are controlled with Labview software in order to get a focused spot at the surface of the semiconductor in the range of 60 µm in diameter. The high voltage device under test (DUT) is placed in the vacuum chamber as shown in Fig. 2 and reverse biased with a FUG (up to 12.5 kV). The surface of the DUT is scanned in with a step of 10 µm under high voltage. Current is measured with a microammeter (Keithley 6485). It allows to realize mapping of the induced current in both directions (X and Y) or only lines. The intensity of the spectra is related to the electric field and hence to the reverse voltage applied to the DUT. Thanks to the simulation software, it is possible to have a correlation with the electric field inside the device. The OBIC principle has already been described elsewhere in [9][10].

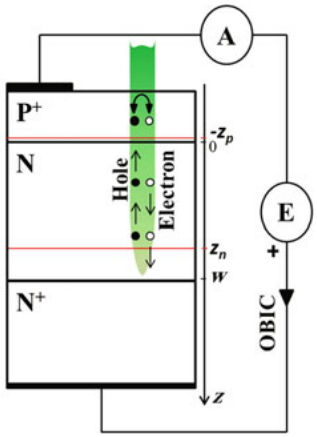

Fig. 1: Reverse-biased plane-parallel infinite PN junction

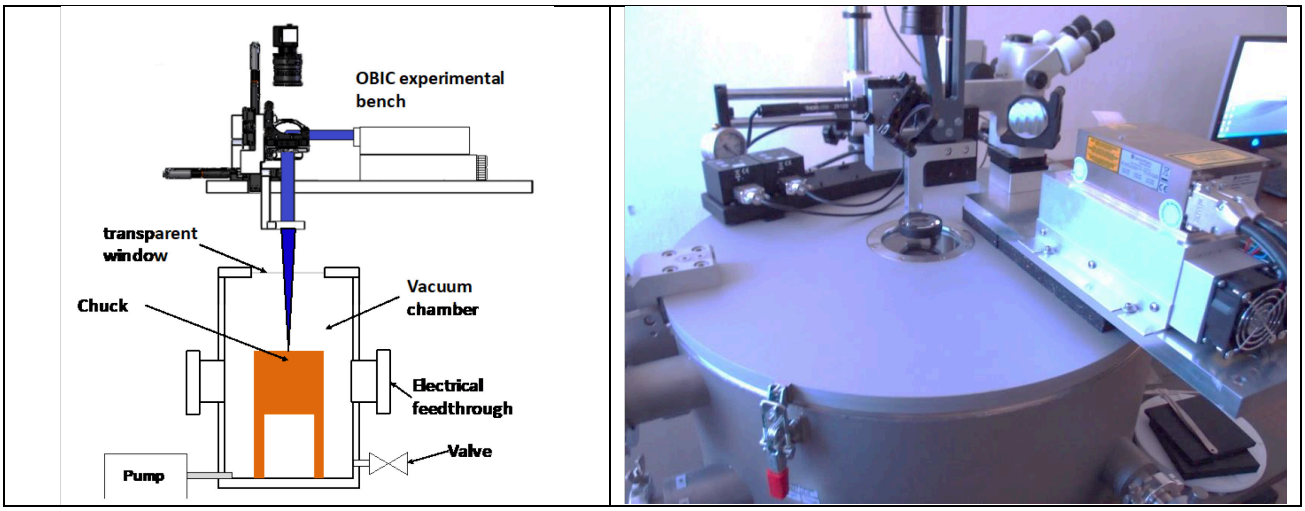

Fig. 2: Experimental OBIC bench (schematic on the left and picture on the right).

Two different wavelengths could be used either the green one with λ=532 nm or the UV with λ=349 nm, supplied with two pulsed semiconductor lasers. Two different workbenches have been developed.

3 - Simulation of OBIC structure

TCAD is used to describe the structure. (Finite element method) Reference to Synopsys [11].

TCAD allows to model the experimental results, and hence to know the electric field strength. Physical parameters of the semiconductor is taken into account, but also the geometrical parameters of the beam (diameter, spatial gaussian distribution).

4 - Measurement on 4H-SiC PiN diodes

A great number of structures have been studied, mostly with the aim to reach high voltage device. The first range is about a voltage capability of 3300V with bipolar diode.

4.1 Medium voltage PiN diode (3.3 kV class).

Single JTE bipolar diode with two doses have been measured as described in table 1. A cross-section of the diode is shown in Fig. 3.

	Device 1	Device 2
JTE dose [cm^{-2}]	1.23×10^{13}	6.84×10^{12}
Epilayer thickness [µm]	40	30

Table 1: Details of the 2 doses and thicknesses

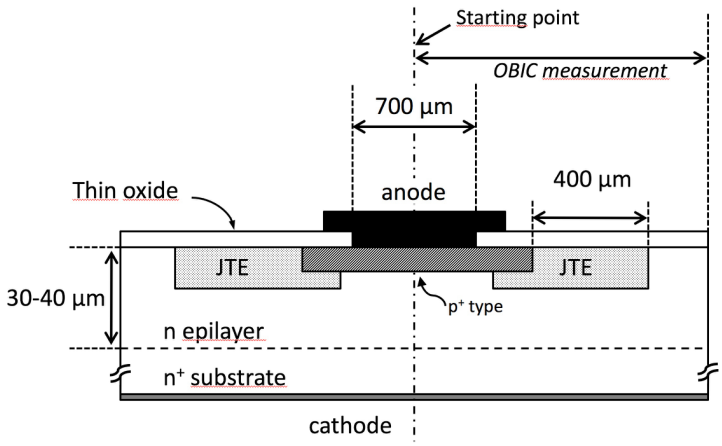

Fig. 3: Cross section of the PiN JTE protected diode

OBIC measurements have been performed on both devices namely device 1 and device 2 with the UV-laser. Applied reverse voltages range between 800 and 2850V depending of the breakdown voltage. For device 1 with the highest JTE dose, the increase of the obic current is located near the edge of the JTE. On the contrary, with device 2, the lowest JTE dose, the increase of the obic current is located near the P+/JTE area, as it could be observed on the Figure 4. Location of the metallization, P+ and JTE areas are mentioned at the bottom of the graphs.

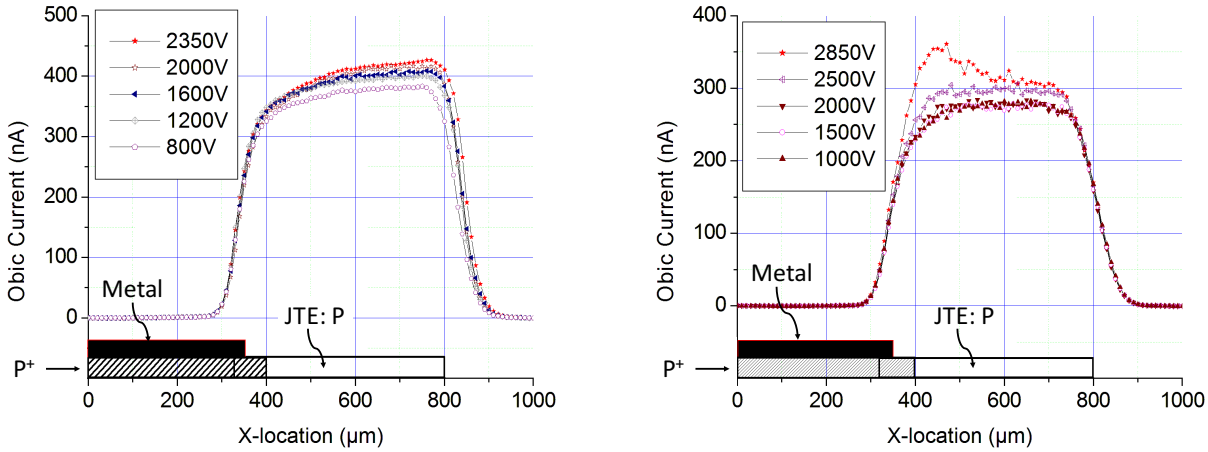

Fig. 4. OBIC current measured at different increasing voltages on device #1 (left) and device #2 (right).

Near breakdown voltage induces high electric field, which leads to an increase of the OBIC signal.

4.2 High voltage PiN diode (10 kV class).

High voltage PiN diodes were fabricated on a 4H-SiC wafer using a 110 µm thick epilayer with a doping concentration of 7×10^{14} cm^{-3}. These diodes are MESA-JTE protected with or without JTE-ring (6 or 8 rings), as shown in Fig. 5.

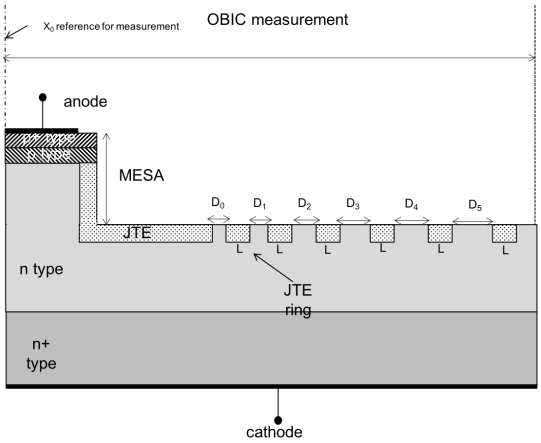

Fig. 5. Cross section of the right half part of high voltage bipolar PiN diode MESA protected with 6 JTE rings.

Prior to OBIC measurements, reverse IV characteristics were performed to determine the near breakdown voltage. High voltage OBIC measurements were performed in 1D-sweeping mode with a step of 10 µm for increasing voltages. 4 kinds of diodes were measured (400 µm JTE length, 500 µm JTE length, 400 µm JTE length with 6 JTE-rings and finally 400 µm JTE length with 8 JTE-rings).

As the voltage increases, and is near the breakdown voltage, one can observe the birth of an OBIC peak located near the P+/JTE area in Figure 6 to 9. This is due to the electric field enhancement at the P^+/JTE overlap, meaning that the JTE dose is too low. Moreover breakdown voltages are far from the theoretical breakdown voltage (10 kV) and the impact of the protection is not very clear.

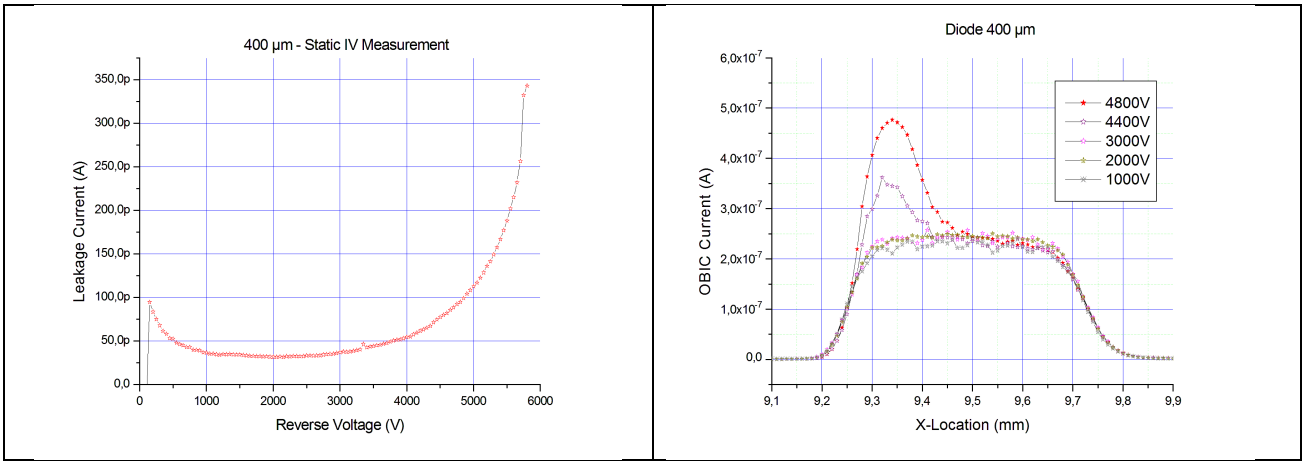

Fig. 6. IV characteristics (left) and 1D-sweeping OBIC measurements (right) on diode **400 µm** MESA JTE protected

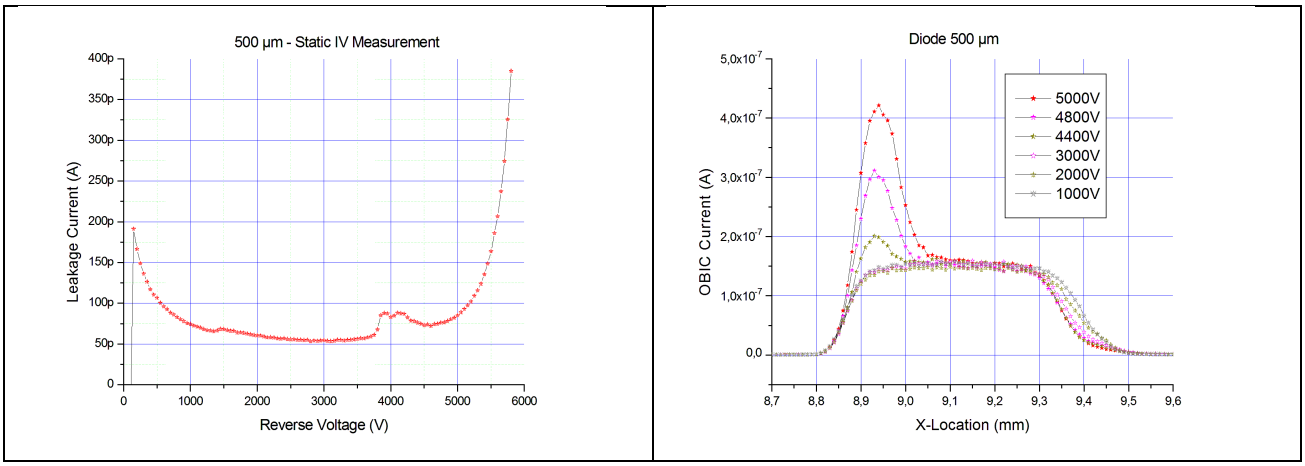

Fig. 7. IV characteristics (left) and 1D-sweeping OBIC measurements (right) on diode **500 µm** MESA JTE protected

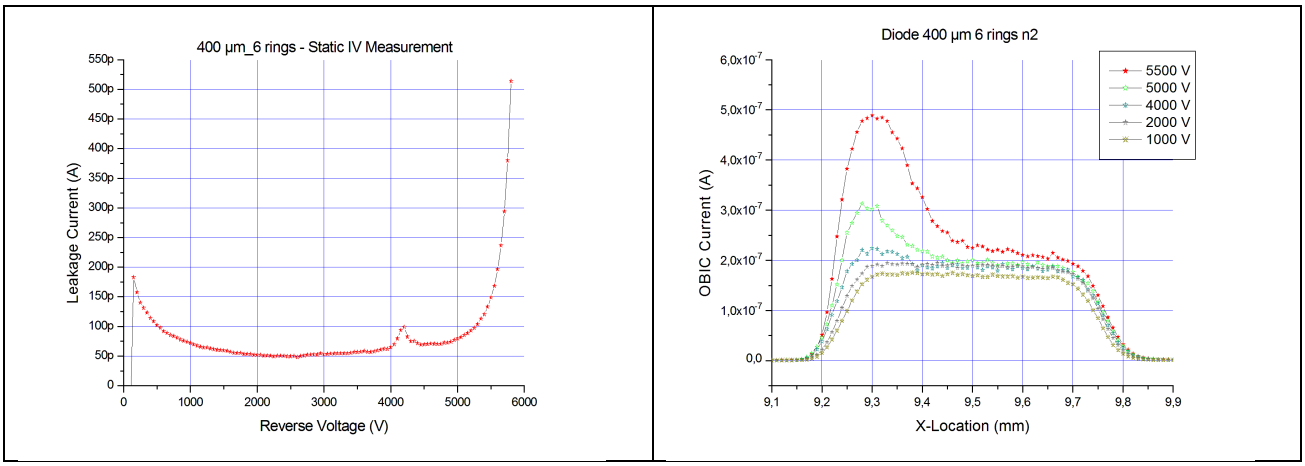

Fig. 8. IV characteristics (left) and 1D-sweeping OBIC measurements (right) on diode **400 µm – 6 rings** MESA JTE protected

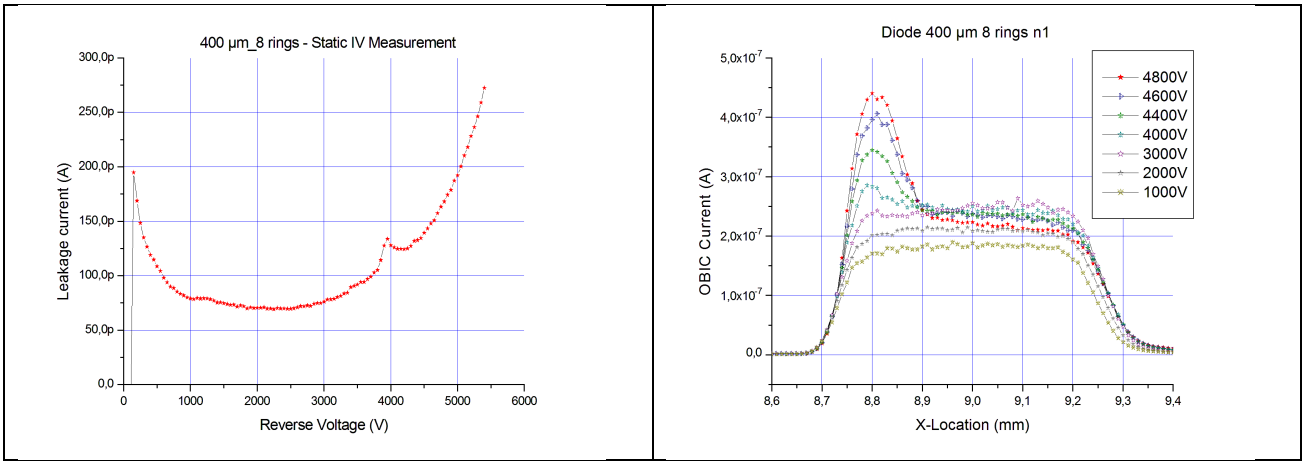

Fig. 9. IV characteristics (left) and 1D-sweeping OBIC measurements (right) on diode **400 µm – 8 rings** MESA JTE protected

The following figures show the evolution in 2D of the OBIC current for six different voltages (0, 2000V, 3500V 3800V 4000 and 4400V) on the diode 400 µm – 8 rings MESA JTE protected. The OBIC current is normalized to the maximum value found for each cartography. The full diode is scanned with a step of 100 µm in both directions. Lack of OBIC signal on the upper part of each mapping is due to shadow of the connecting probe. As the reverse bias increases, one can observe the birth of a peak value at on edge of the periphery (V_R>3500V) and then the complete side (V_R=4400V). These mappings give more information than the 1D-sweeping, but are more time-consuming.

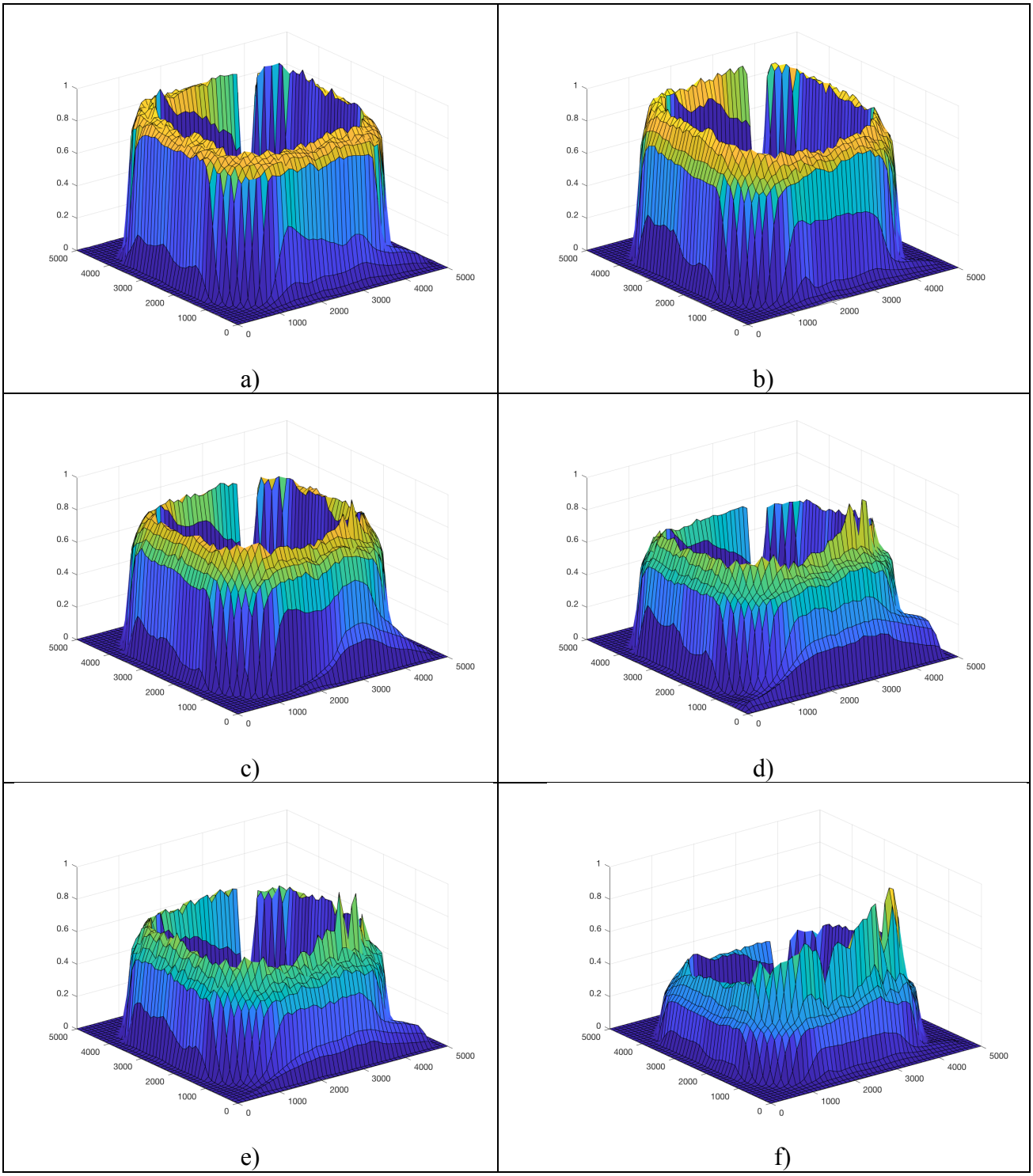

Fig 10. 2D-mapping of the OBIC current versus different voltages a) 0V, b) 2000V, c) 3500V, d) 3800V, e) 4000V and f) 4400V) for the diode 400 µm JTE length with 8 JTE-rings.

5 - Measurements on other wide bandgap semiconductor samples

Test measurements have been performed using the UV-Laser on GaN and Diamond devices. Two-photons absorption process takes place because the photon energy (E_φ=hc/λ) is smaller than the bandgap energy (E_G).

5.1 GaN Schottky diodes

OBIC measurements have been realized on GaN Schottky on test structure as shown in Fig. 11. Structures were low reverse biased. Current collapse in the GaN devices prevent high speed OBIC measurements: a delay is required after illumination by the optical beam for detrapping the traps in the

material. 10 seconds were delayed after each measurement of the current before moving the spot location.
Figure 11 shows 1D-OBIC scan for low reverse voltage (V_R = 10 V). Results show an OBIC signal appearing at both edges of the MESA.

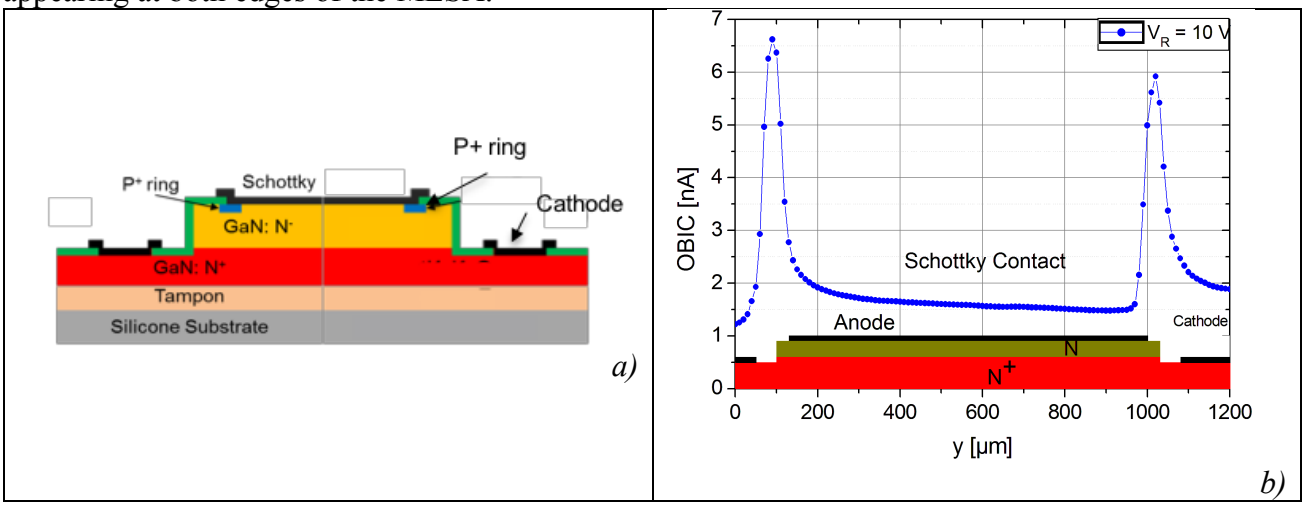

Fig. 11: Cross section a) and 1D-OBIC scan b) on Schottky GaN diode for a reverse voltage of 10 V using the UV laser.

5.2 Diamond Schottky diodes

OBIC measurements under low voltage biasing ((V_R = 10 V) have also been performed on Schottky diamond diodes with the UV laser source as shown in Fig 12. The circular shape (150 µm in diameter) of the device is clear; one can observe also the signal under the metallization due to the very small thickness of the metal on top of the diode (transparency effect).

The bandgap of the diamond (5.45 eV) is larger than the photon energy (E_φ=hc/λ=3.56 eV) and hence the two-photon absorption process takes place in this case. As for the GaN diode, a delay of 10 s is applied before the displacement of the laser beam location.

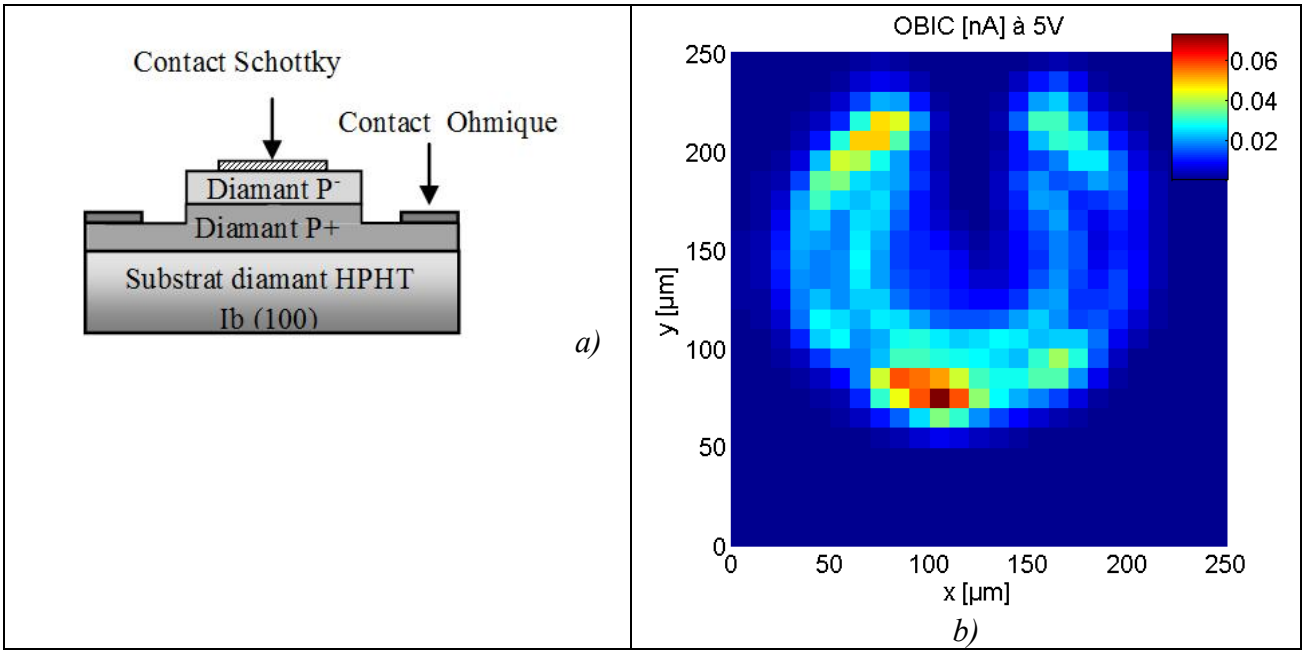

Fig. 12: Cross section a) and 2D-OBIC cartography b) on Schottky diamond diode for a reverse voltage of 5 V using the UV laser (diameter of the diode is 150 µm).

6 - Opportunities offered from OBIC

6.1 - Ionization coefficients determination

As it was shown in the Simulation section, the determination of ionization rates is essential to predict breakdown voltage of devices. OBIC method is used to determine multiplication coefficient M which is defined as the ratio between OBIC and a voltage V and a reference voltage V_0 (where there is no multiplication). Eq. 1 shows the expression of M.

$$M(V) = \frac{OBIC(V)}{OBIC(V_0)} = \frac{M_n J_n(z_p) + M_p J_p(z_n) + M_{SCR} J_{SCR}}{OBIC(V_0)} \qquad Eq.\ 1$$

where M_n (M_p, M_{SCR}) is electron (hole, SCR) multiplication coefficient, J_n and J_p are minority carrier currents at the edges of the SCR, J_{SCR} is the photo-generated current inside the SCR (figure 1). M_n, M_p, M_{SCR} depend on the ionization rates, their expressions are given in [12]. Ionization rates α_p (for holes) and α_n (for electrons) are given by Eq. 2 [13].

$$\alpha_{n,p} = A_{n,b}\, exp\left(-{}^{B_{n,p}}/_{E}\right) \qquad Eq.\ 2$$

where $A_{n,b}$ and $B_{n,p}$ are constants to be determined and E is the electric field.
OBIC measurements are realized on Schottky diodes with an optical window. Experimental multiplication curve (inside the optical window) is found by considering V_0 = 1 V. Ionization rates parameters are then adjusted to fit theoretical curve of M with experimental one by minimizing an error function ΔM [12, 14]. Table 2 displays the values of $A_{n,b}$ and $B_{n,p}$ for 4H-SiC using both of laser sources (and then single- and two-photon absorption processes). Figure 13 shows ionization rates vs. the inverse of electric field for 4H-SiC. Comparison shows that the curves are close when using green or UV laser.

	UV laser	**Green laser**	**Experimental**
A_n [10^6 cm^{-1}]	0.99	1.11	
B_n [10^7 V.cm^{-1}]	1.29	1.22	
A_p [10^6 cm^{-1}]	1.61	1.71	
B_p [10^7 V.cm^{-1}]	1.15	1.18	
ΔM	1.824	0.724	
V_{BR} [V]	62.2	59.2	58.8
E_C [MV.cm^{-1}]	4.9747	4.9036	

Table 2. Parameters of ionization rates of 4H-SiC using OBIC method with two different wavelengths [12, 14].

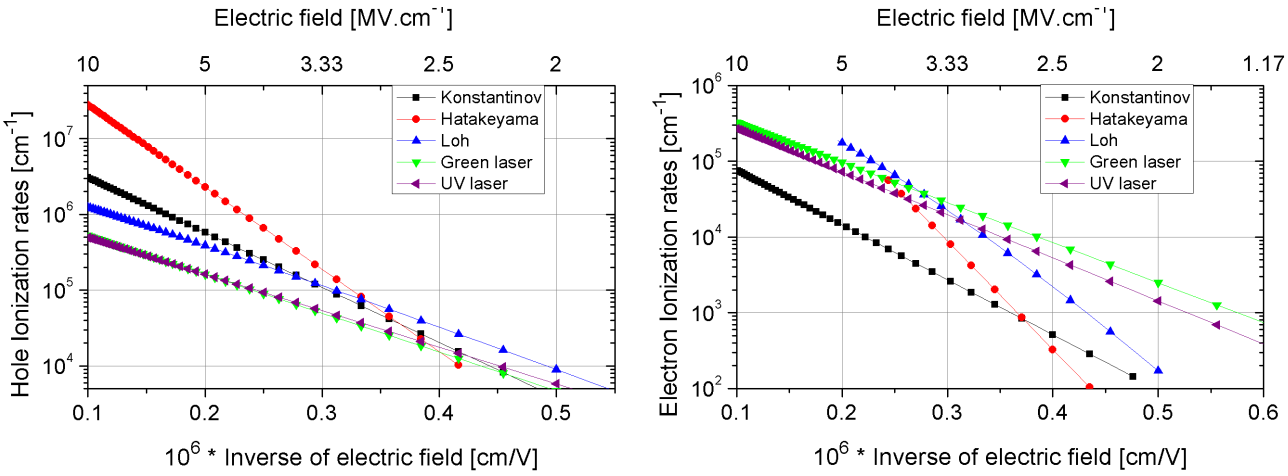

Fig. 13. Ionization rates a) hole and b) electron vs. inverse of electric field for 4H-SiC using OBIC method with single- and two-photon absorption process, and compared to other authors.

Comparison shows that the hole's ionization rates α_p are greater than electron's ionization rates α_n (as the other authors) but the ratio α_p/α_n is about twice. Difference found between the authors is due to the doping levels of DUTs and the method used to extract ionization rates.

6.2 Lifetime extraction

Lifetime of charge carriers is a key parameter for power devices, it allows to predict the static and dynamic losses of a junction. OBIC technique was used to determine minority carrier lifetime in 4H-SiC [15]. OBIC measurements were performed on JTE (200 µm long) protected PiN diode. At the edge of the JTE layer, the junction is supposed to be vertical, and the minority charge carriers are holes. When the laser beam scans the diode, the OBIC measured at the edge of the JTE decreases as a function of the minority carrier diffusion length L_{dp} as shown in Eq. 3.

$$OBIC(x) = u\,exp\left(-\frac{x}{L_{dp}}\right) \qquad Eq.\ 3$$

where u is the optical generation rate.

Minority carrier lifetime τ_p is related to L_{dp} and the diffusion coefficient of holes D_p as shown in Eq. 4.

$$\tau_p = \frac{{L_{dp}}^2}{D_p} = \frac{q{L_{dp}}^2}{kT\mu_p} \qquad Eq.\ 4$$

where k is Boltzmann constant, T the temperature, q the electron charge and μ_p the hole mobility.

Figure 14 shows the logarithm of OBIC ln(OBIC) vs. the beam position signal for voltages between 0 and 700 V. Referring to Eq. 4, this value is the inverse of L_{dp}, so the diffusion length of holes is then 14.7 µm. Using Eq. 4 with hole mobility of 115 $cm^2.V^{-1}s^{-1}$, the lifetime of holes found is 730 ns.

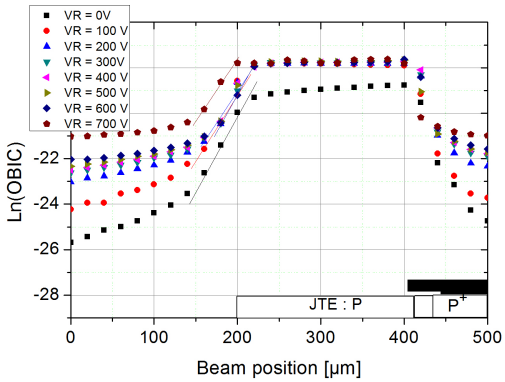

Fig. 14. ln(OBIC) vs. the beam position for $0 \leq V_R \leq 700$ V.

6.3 Defect near the surface (Green laser mapping)

OBIC measurements allow the detection of material defects, assuming that a defect is shown as a local variation of electric field. Figure 15 shows 2D-OBIC measurements on a diode with a defect located in the JTE area. This diode has a breakdown voltage of 300 V. A local OBIC peak appears at the defect position, so OBIC technique is a non-destructive method to determine defects.

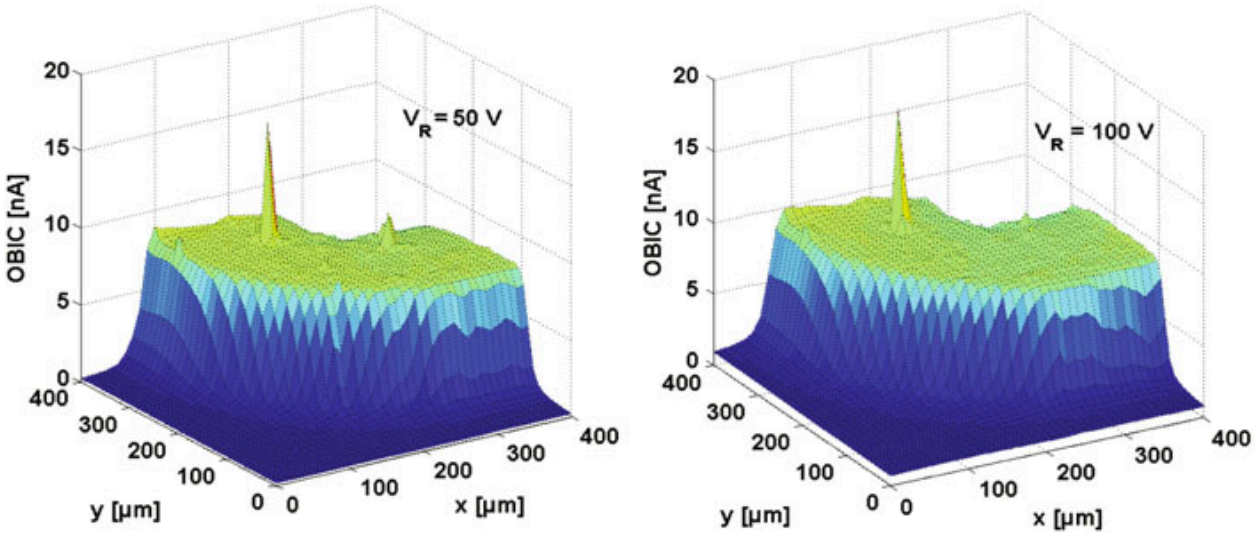

Fig. 15. 2D-OBIC cartography on b-structure diode presenting a local defect using the green laser.

Conclusions

High voltages OBIC measurements have been realized in this paper.

Next step of this research work will focus on the reduction of the size of the beam, so that small geometries could be clearly distinguished.

It has been shown that OBIC measurements are possible with WBG materials. Single or two-photon absorption process is chosen adequately. It is now open to other semiconductors.

Acknowledgments

The authors would like to thank **SuperGrid Institute** (SGI) for providing high voltage SiC devices, **Diamonix** research program for providing Diamond diode, **Tours 2015** research program for providing GaN devices and finally for financial support the Caisse des Dépôts et Consignations (CDC) and BPI-France (FilSiC: Convention n°O13953-410188).

References

[1] K. Shenai, R. Scott, B.J. Baliga, "Optimum Semiconductors for high-power electronics" IEEE Transactions on Electron Devices, Vol. 36, n°9, 1989, pp. 1811-1823

[2] C. Raynaud, D. Tournier, H. Morel, D. Planson, "Comparison of high voltage and high temperature performances of wide bandgap semiconductors for vertical power devices" Diamond & Related Materials vol.19 (2010) p. 1-6.

[3] T. Mizushima, K. Takenaka, H. Fujisawa, T. Kato, S. Harada, Y. Tanaka, M. Okamoto, M. Sometani, D. Okamoto, N. Kumagai, S. Matsunanaga, T. Deguchi, M. Arai, T. Hatakeyama, Y. Makifuchi, T. Araoka, N. Oose, T. Tsutsumi, M. Yoshikawa, K. Tatera, A. Tanaka, S. Ogata, K. Nakayama, T. Hayashi, K. Asano, M. Harashima, Y. Sano, E. Morisaki, M. Takei, M. Miyajima, H. Kimura, A. Otsuki, Y. Yonezawa, K. Fukuda, H. Okumura and T. Kimoto, "Dynamic Characteristics of large current capacity module using 16-kV Ultrahigh voltage SiC Flip-type n-channel IE-IGBT" Proc. Int. Symp. On Power Semiconductor Devices & IC's, 2014, pp 277-280

[4] J. Millán, P. Godignon, X. Perpiñà, A. Pérez-Tomás, J. Rebollo, "A Survey of Wide Bandgap Power Semiconductor Devices" IEEE Transactions on Power Electronics Year: 2014, Volume: 29, Issue: 5 Pages: 2155 - 2163

[5] K. Fukuda, D. Okamoto, M. Okamoto, T. Deguchi, T. Mizushima, K. Takenaka, H. Fujisawa, S. Harada, Y. Tanaka, Y. Yonezawa, T. Kato, S. Katakami, M. Arai, M. Takei, S. Matsunaga, K. Takao, T. Shinohe, T. Izumi, T. Hayashi, S. Ogata, K. Asano, H. Okumura, T. Kimoto,

"Development of Ultrahigh-Voltage SiC Devices" IEEE Transactions on Electron Devices, 2015, Volume: 62, Issue: 2, Pages: 396 – 404

[6] N. Kaji, H. Niwa, J. Suda, T. Kimoto, "Ultrahigh-Voltage SiC p-i-n Diodes With Improved Forward Characteristics", IEEE Transactions on Electron Devices, 2015, Volume: 62, Issue: 2, Pages: 374 – 381

[7] R. Perret, Power Electronics Semiconductor Devices, Ed. Wiley-ISTE, 2009, ISBN: 978-1-848-21064-6.

[8] W. J. Choyke, H. Matsunami, G. Pensl, Silicon Carbide: Recent Major Advances, Ed. Springer Science & Business Media, 2003, ISBN: 978-3-642-18870-1.

[9] C. Raynaud, D.-M. Nguyen, N. Dheilly, D. Tournier, P. Brosselard, M. Lazar, D. Planson « Optical beam induced current measurements: principles and applications to SiC device characterization », Phys. Status Solidi A 206, n°10, 2273-2283 (2009) / doi: 10.1002/pssa.200825183

[10] D. Planson, P. Brosselard, K. Isoird, M. Lazar, L.-V. Phung, C. Raynaud, D. Tournier, Wide Bandgap Semiconductors for Ultra-High Voltage Devices. Design and characterization aspects. CAS Conference Sinaia - Romania 13-15 Octobre, 2014 (doi:http://dx.doi.org/10.1109/SMICND.2014.6966383).

[11] Sentaurus Device User Guide 2017 Version N. Website: http://www.synopsys.com/home.aspx

[12] H. Hamad, C. Raynaud, P. Bevilacqua, S. Scharnholz, D. Planson « Temperature dependence of 4H-SiC ionization rates using Optical Beam Induced Current », Mater. Sci. Forum 821-823, 2015, pages 223-228

[13] A. G. Chynoweth « Uniform Silicon p-n junctions. Ionization Rates for Electrons », J. Appl. Phys., 1960, Vol. 31, page 1161.

[14] H. Hamad, C. Raynaud, P. Bevilacqua, S. Scharnholz, B. Vergne, D. Planson « Determination of 4H-SiC ionization rates using OBIC based on two-photon absorption », Mater. Sci. Forum 858, 2016, pages 245-248

[15] T. Flohr and R. Helbig, "Determination of minority-carrier lifetime and surface recombination velocity by Optical-Beam-Induced-Current measurements at different light wavelengths," J. Appl. Phys., 1989, Vol. 66, Issue 7, pp. 3060-3065.